Journal of Materials Chemistry

Cite this: J. Mater. Chem., 2012, 22, 2844

www.rsc.org/materials

COMMUNICATION

Self-assembly of ultrathin porous NiO nanosheets/graphene hierarchical structure for high-capacity and high-rate lithium storage†

Yun Huang,‡[ac] Xiao-lei Huang,‡[ab] Jian-she Lian,[c] Dan Xu,[a] Li-min Wang[a] and Xin-bo Zhang*[a]

Received 14th November 2011, Accepted 19th December 2011
DOI: 10.1039/c2jm15865e

A unique ultrathin porous NiO nanosheets/graphene hierarchical structure is successfully fabricated *via* a facile, effective, and general strategy. The advantageous combination of conducting and flexible graphene and porous and ultrathin NiO nanosheets endows the obtained hybrid with a remarkable lithium-storage performance, including high reversible capacity, good rate capability and cycle performance.

The ever-growing demand for large-scale energy storage applications such as alternative energy and electric transportation has triggered significant research efforts on high-energy and power-density lithium-ion batteries (LIBs).[1] There is a general consensus that the breakthrough of energy density necessarily requires passage from classical intercalation reactions to conversion reactions.[2] However, even after a decade of intensive efforts, the terrible capacity degradation still greatly hampers the application of conversion-based materials.[1a,2b,3] On the other hand, for achieving a high power density, although many strategies such as downsizing the electrode materials to nanoscale, coating or mixing with more conductive materials, and doping with foreign atoms have been developed to obtain rapid ionic and electronic diffusion in electrode materials, these methods suffer from more or less severe drawbacks such as poor cycling stability and the requirement of a high percentage of carbon black.[4] Therefore, there is an urgent need to simultaneously improve cycling stability, energy- and power-density of LIBs.

Nickel oxide (NiO), as one of the most important family of functional inorganic materials, has numerous applications in the field of catalysis,[5a] gas sensors,[5b] magnetic materials,[5c] as well as promising anode materials[5d–g] for LIBs due to its abundance, low cost, and high theoretical capacity (717 mA h g^{-1}). However, like other conversion-based anode materials, its implementation to LIBs is greatly hindered by its poor cycling and rate performances.[5e,f] To circumvent these obstacles, one of the most promising strategies is to construct hybrid materials with fascinating graphene,[6] possessing high surface area, superior electrical conductivity and excellent mechanical flexibility.[7] Unfortunately, the electroactive nanoparticles (NPs) are still prone to aggregation upon cycling because of non-intimate contact between graphene layers and the electroactive NPs, which would lead to a serious decrease in capacity of the metal oxide/graphene composites.[8] Therefore, development of a facile and general strategy to substantially enhance the cycling stability and rate performance of metal oxide is of great importance.

In contrast to small and isolated 0D spherical NPs, when electroactive materials are in large area 2D, ultrathin and porous nanosheets structure and successfully self-assembled with graphene sheets (GNS), the relative immobility and facile strain relaxation of large area 2D structure would greatly alleviate the aggregation of electroactive materials, and moreover, the ultrathin and porous structure would improve the structural stability against volume expansion, which would theoretically benefit the cycling stability. Even more important, the unique hierarchical structure could also offer substantial improvement in power and energy density over bulk electrodes stemming from the following advantages: (1) the 2D geometry together with the ultrathin and porous structure would offer sufficient contact interface between active materials and electrolytes; (2) the ultrathin and porous structure is of benefit to fast Li^+ transfer; (3) the large area of conducting graphene offers continuous and fast conducting pathways for electrons through the electrodes. Although assembly of 0D spherical NPs with graphene has been widely shown,[6a–e,8a,b] there are few reports on active materials with different morphologies such as 2D morphology,[5f,9] to say nothing of with ultrathin porous nanosheets structure. Thereafter, it remains unexplored and highly desirable to develop a facile and effective strategy to fabricate ultrathin porous NiO nanosheets/graphene (NiO/GNS) hierarchical structure to achieve excellent lithium storage, cycling and rate performance.

Herein, a unique NiO/GNS hierarchical structure is successfully prepared by a facile, effective, and general route. The advantageous combination of ultrathin, porous and large area 2D structure and conductive graphene endows the as-prepared hierarchical structure a good performance of stable and high reversible discharge capacity up to 1098 mA h g^{-1} even after 50 cycles at a current density of

[a]*State Key Laboratory of Rare Earth Resource Utilization, Changchun Institute of Applied Chemistry, Chinese Academy of Sciences, Changchun, 130022, China. E-mail: xbzhang@ciac.jl.cn; Fax: +86-431-85262235; Tel: +86-431-85262235*
[b]*Graduate University of Chinese Academy of Sciences, Beijing, 100049, China*
[c]*Key Laboratory of Automobile Materials, Ministry of Education, and School of Materials Science and Engineering, Jilin University, Changchun, 130012, China*

† Electronic supplementary information (ESI) available: Experimental section and supplementary figures. See DOI: 10.1039/c2jm15865e

‡ Yun Huang and Xiao-lei Huang contributed equally to this work.

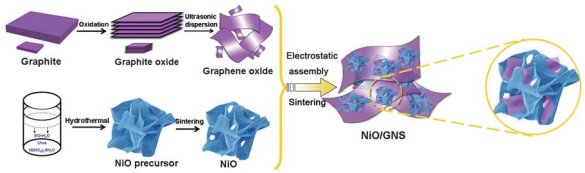

Scheme 1 Illustration of the procedures for preparation of NiO/GNS hierarchical structure.

100 mA g^{-1}, and a good rate capability of 615 mA h g^{-1} at a high current density of 4 A g^{-1}, which opens up new opportunities in the development of high performance next-generation LIBs.

The formation procedures of NiO/GNS hierarchical structure are illustrated in Scheme 1. Briefly, a hydrothermal process is proposed to synthesize self-assembled ultrathin NiO precursor, wherein ethylene glycol is employed as a structure directing agent. Then the obtained NiO precursor is thermally decomposed to porous NiO through sintering in air. The NiO/GNS hierarchical structure is prepared by electrostatic interaction between positively charged NiO nanosheets and negatively charged graphene oxide in aqueous solution with a pH = 4 and then sintering in Ar gas atmosphere (Fig. S1, ESI†). The NiO/GNS hierarchical structure is stable, possibly due to the intermolecular force of NiO and GNS instead of the chemical bond (Fig. S2†). It should be noted that the size of the employed graphene oxide should cover the range from the nanoscale to microscale, which is of critical importance for our strategy to ensure that both the self-assembled NiO and its corresponding nanosheet can be effectively covered or supported by graphene oxide (Fig. S3c†). Importantly, almost all the NiO and graphene oxide are fully assembled to leave an almost transparent aqueous solution (Fig. S4†).

Fig. 1 shows the X-ray diffraction (XRD) pattern of the obtained products. The as-prepared NiO precursor (trace a) can be reasonably assigned to $NiO_{2.45}C_{0.74}N_{0.25}H_{2.90}$.[10] After sintering at 500 °C in air, the XRD pattern changes significantly and all the diffraction peaks can be referenced to a face-centered cubic unit cell with lattice constant a = 4.1946 Å (trace b). The 2θ values of 37.092°, 43.095°, 62.584°, 75.042° and 79.008° can be indexed to diffractions of (111), (200), (220), (311), and (222) planes of NiO, respectively (PDF #65-2901). It should be noted that the crystallinity of NiO/GNS (trace c) becomes better due to further sintering in Ar gas employed to reduce graphene-oxide to graphene.[5f] Remarkably, no conventional stacking peak of graphene sheets at $2\theta = 26.68°$ is detected. Furthermore, as mentioned above, the aqueous solution after assembly is near transparent (Fig. S4†). Thus we can reasonably conclude that almost all the graphene oxide sheets are successfully assembled with NiO, highlighting the efficiency of our proposed strategy. The mass ratio of graphene to NiO in NiO/GNS is determined by thermogravimetric analysis, which turns out to be 13 wt% graphene and 87 wt% NiO (Fig. S5†).

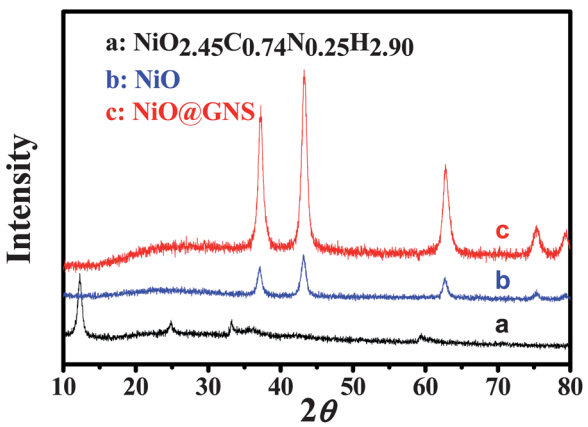

Fig. 1 XRD patterns of (a) $NiO_{2.45}C_{0.74}N_{0.25}H_{2.90}$, (b) NiO nanosheets, and (c) NiO/GNS hierarchical structure.

The morphology and structure of NiO precursor, NiO, and NiO/GNS hierarchical structure are compared by scanning electron microscopy (SEM) and transmission electron microscopy (TEM). It can be found that the as-synthesized NiO precursor shows a self-assembled porous structure (Fig. 2a) which is composed of ultrathin nanosheets (less than 6 nm, Fig. S3a†) with smooth surface (Fig. 2c). Interestingly, after sintering, the ultrathin structure and interspace of self-assembled framework are well maintained (Fig. 2b and S3b†), while the surface of obtained NiO becomes rough (Fig. 2d). The surface area of the obtained NiO is 59.2 m^2 g^{-1} (Fig. S7a†). The magnified TEM image of NiO shows that some favourable hexagonal holes with typical diameters of 15–50 nm formed in the obtained NiO nanosheets (Fig. 2e and S6†). The formation of the hole might be due to the following process. First, ethylene glycol likely plays a critical role as a structure-directing agent to form the defects and sheetlike structure. Then the highly crystallized nickel oxide precursor decomposes and transforms into NiO nanosheets during calcination, and the high reaction/etching rate at the defect sites in the NiO precursor nanosheets leads to the formation of hexagonal holes.[10] Thanks to the favourable electrostatic interaction (Fig. S1†), the

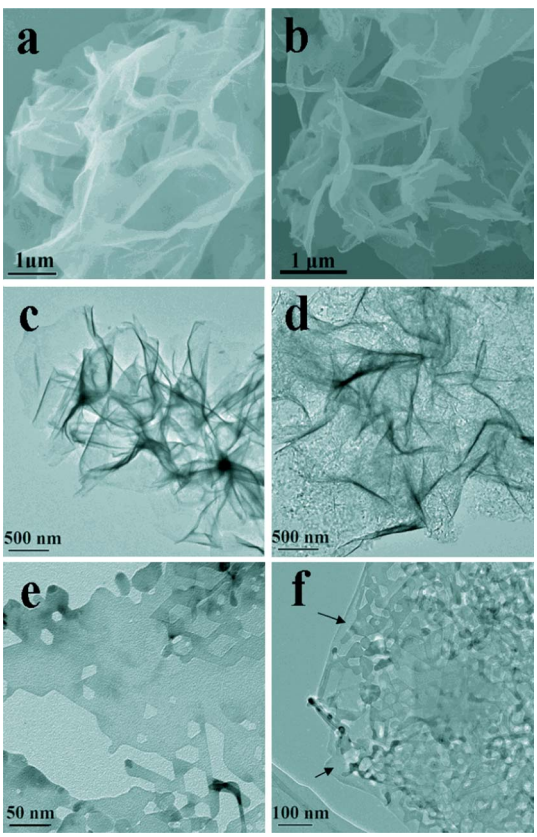

Fig. 2 (a and b) SEM images of NiO precursor and NiO, (c and d) TEM images of NiO precursor and NiO, (e) magnified TEM image of NiO and (f) TEM image of NiO/GNS.

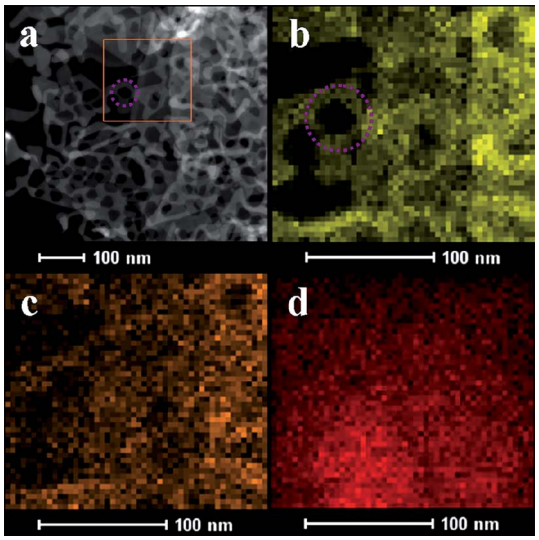

Fig. 3 TEM (a) and EDS characterization of NiO/GNS hierarchical structure: (b) nickel, (c) oxygen, and (d) carbon mapping of the orange boxed region shown in (a).

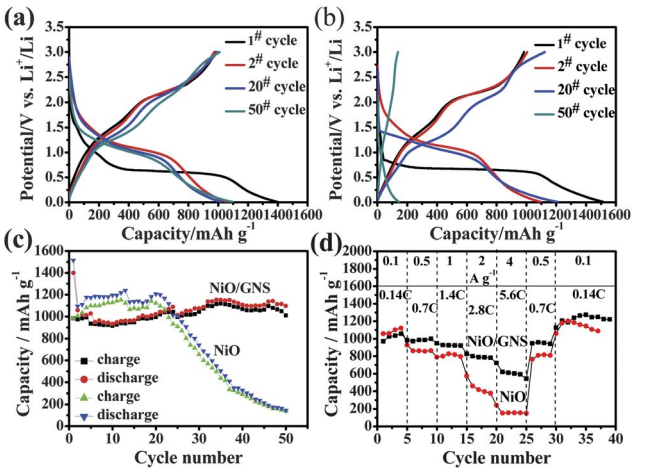

Fig. 4 (a) Galvanostatic charge/discharge profiles of NiO/GNS and (b) NiO nanosheets, (c) cycling performance of NiO/GNS and NiO at a current density of 100 mA g^{-1} (0.14 C), and (d) reversible capacity *vs.* current density (rate capability) for NiO/GNS and NiO. All the half-cells were cycled in the potential window from 0.01 to 3.0 V.

intimate interaction of NiO nanosheets and graphene oxide (Fig. S8a†) would endow the complete and full combination of NiO and GNS to form NiO/GNS hierarchical structure, which is confirmed by the XRD result (*vide supra*) and no graphite particle can be found in the sample (Fig. S8b†). The surface area of the obtained NiO/GNS is 43 m^2 g^{-1}. The existence of GNS can be determined by the graphene structure with few layers observed on the edge of the sample (arrow area in Fig. 2f). The physical and textural properties of all samples can be seen in Table S1†.

To further confirm the hierarchical structure of NiO/GNS, dispersive spectroscopic (EDS) mapping is employed (Fig. 3 and S9†). As expected, the existence and distribution of Ni (Fig. 3b), O (Fig. 3c) and C (Fig. 3d) unanimously confirm the intimate coexistence of graphene and NiO (Fig. 3a). This favorable structure could be helpful for preventing aggregation or restacking of graphene nanosheets and ultrathin porous NiO nanosheets upon cycling. Moreover, as an ideal electron conductor, graphene would play an important role as a conductive network within the electrode, which would benefit the electrochemical performance (*vide infra*). In addition, the purple circled region in Fig. 3a shows a hexagonal structure without Ni distribution, confirming again the existence of hexagonal holes.

Coin cells with a metallic lithium anode are assembled to investigate the electrochemical performance of the NiO and NiO/GNS composite. Strikingly, a large specific discharge capacity of 1398 mA h g^{-1} and a reversible capacity of 982 mA h g^{-1} are achieved for NiO/GNS (Fig. 4a) at a current density of 100 mA g^{-1} (0.14 C), which represents almost four times that of the gravimetric capacity (372 mAh g^{-1}) of the state-of-the-art graphite materials and thus greatly expands the range of anode choices. An irreversible capacity of 416 mA h g^{-1} during the first discharge/charge process might be attributed to the formation of the solid electrolyte interface (SEI) film at the electrode/electrolyte interface and the reaction of residual oxygen-containing functional groups on graphene with lithium ions. It should be pointed out that the coulombic efficiencies (Fig. 4c) increase to almost unity at successive cycles, indicating that the formed SEI during the first cycle is favourable and stable. For comparison, bare NiO nanosheets are also tested under the same electrochemical conditions (Fig. 4b). Although the initial discharge capacity (1515 mA h g^{-1}) is higher than that of NiO/GNS, its columbic efficiency (65%) is lower than that of NiO/GNS (71%). The fact that the capacity of NiO is higher than that of NiO/GNS for the 1st cycle is caused by the much lower capacity of graphene compared to NiO (Fig. S10†). The cyclic voltammetry (CV) is employed to clarify the energy storage redox mechanism of the NiO/GNS composite (Fig. S11a and b†). After 50 cycles (Fig. 4c), the reversible capacity of NiO decreases to only 145 mA h g^{-1}, which is more than seven times lower than that of the devices fabricated by the NiO/GNS electrode (1098 mA h g^{-1}). In addition, the reversible retention capacity of the NiO/GNS electrode (112%) after 50 cycles is much higher than that of the NiO electrode (15%). The inferior cycling performance of bare NiO should be caused by its large volume changes, poor electric conductivity and aggregation of NiO. In contrast, in the NiO/GNS hierarchical structure, the excellent flexibility and conductivity of graphene can not only buffer the volume change but also prevent the aggregation of active materials from disconnecting the current collector.

Fig. 4d demonstrates the rate capability of NiO and NiO/GNS electrodes from current densities of 0.1 A g^{-1} (0.14 C) to 4 A g^{-1} (5.6 C) for five cycles at each current density. At the low current density (0.14 C), the capacities of NiO and NiO/GNS are comparable and NiO is even a little advantageous. However, this situation reverses when the current density is increased. For example, in the current density of 5.6 C, the NiO/GNS composite is still able to deliver a discharge capacity of 615 mA h g^{-1}, which is much higher than that of NiO (165 mA h g^{-1}). The improved rate performance of the NiO/GNS hybrid could be reasonably attributed to advantageous combination of the highly conductive graphene and ultrathin and porous structure of NiO, which provides a sufficient electrode/electrolyte contact area and facilitates continuous and fast conducting pathways for electrons through the electrodes during the lithiation/delithiation process. The greatly improved electrical conductivity of NiO/GNS composites compared to that of NiO is shown in Table S1†. Meanwhile, the electrochemical impedance spectra of NiO and

NiO/GNS composites also confirmed that the assembly with graphene largely improves the electrochemical activity of the as-obtained NiO (Fig. S11c†).

In summary, we have demonstrated a facile, effective and general strategy to successfully fabricate ultrathin porous NiO/GNS hierarchical structure. Interesting, in contrast to bare NiO, the as-prepared NiO/GNS composite shows a significantly improved cycle life and rate capacity than that of the bare NiO, which is primarily attributed to the advantageous combination of conducting graphene and ultrathin and porous NiO, highlighting the effectiveness and value of our proposed protocol. The obtained good performance opens up new opportunities in the development of high performance next-generation LIB used for alternative energy and electric transportation.

This work is financially supported by 100 Talents Programme of The Chinese Academy of Sciences, National Natural Science Foundation of China (grant no. 21101147), and the Jilin Province Science and Technology Development Program (grant no. 20100102 and 20116008).

Notes and references

1 (*a*) M. Armand and J. M. Tarascon, *Nature*, 2008, **451**, 652; (*b*) B. L. Ellis, K. T. Lee and L. F. Nazar, *Chem. Mater.*, 2010, **22**, 691; (*c*) C. M. Park, J. H. Kim, H. Kim and H. J. Sohn, *Chem. Soc. Rev.*, 2010, **39**, 3115; (*d*) F. Cheng, J. Liang, Z. Tao and J. Chen, *Adv. Mater.*, 2011, **23**, 1695; (*e*) A. Manthiram, *J. Phys. Chem. Lett.*, 2011, **2**, 176; (*f*) H. G. Zhang, X. D. Yu and P. V. Braun, *Nat. Nanotechnol.*, 2011, **6**, 277; (*g*) S. W. Lee, N. Yabuuchi, B. M. Gallant, S. Chen, B. S. Kim, P. T. Hammond and S. H. Yang, *Nat. Nanotechnol.*, 2010, **5**, 531.

2 (*a*) F. Cheng, J. Liang, Z. Tao and J. Chen, *Adv. Mater.*, 2001, **23**, 1695; (*b*) J. Cabana, L. Monconduit, D. Larcher and M. R. Palacin, *Adv. Mater.*, 2010, **22**, E170; (*c*) P. Poizot, S. Laruelle, S. Grugeon, L. Dupont and J. M. Tarascon, *Nature*, 2000, **407**, 496; (*d*) H. L. Wang, L. F. Cui, Y. Yang, H. S. Casalongue, J. T. Robinson, Y. Liang, Y. Cui and H. J. Dai, *J. Am. Chem. Soc.*, 2010, **132**, 13978; (*e*) L. Ji, Z. Tan, T. R. Kuykendall, S. Aloni, S. Xun, E. Lin, V. Battaglia and Y. Zhang, *Phys. Chem. Chem. Phys.*, 2011, **13**, 7170; (*f*) M. G. Kim and J. Cho, *Adv. Funct. Mater.*, 2009, **19**, 1497.

3 (*a*) H. X. Yang, J. F. Qian, Z. X. Chen, X. P. Ai and Y. L. Cao, *J. Phys. Chem. C*, 2007, **111**, 14067; (*b*) Y. Xu, L. Zheng, C. Z. Wu, F. Qi and Y. Xie, *Chem.–Eur. J.*, 2011, **17**, 384; (*c*) H. X. Ji, X. L. Wu, L. Z. Fan, C. Krien, I. Fiering and Y. G. Guo, *Adv. Mater.*, 2010, **22**, 4591; (*d*) W. W. Zhou, C. N. Cheng, J. P. Liu, Y. Y. Tay, J. Jiang, X. T. Jia, J. X. Zhang, H. Gong, H. H. Hng, T. Yu and H. J. Fan, *Adv. Funct. Mater.*, 2011, **21**, 2439.

4 (*a*) X. L. Wu, L. Y. Jiang, F. F. Cao, Y. G. Guo and L. J. Wan, *Adv. Mater.*, 2009, **21**, 2710; (*b*) B. Kang and G. Ceder, *Nature*, 2009, **458**, 190; (*c*) S. Y. Zhan, G. Chen, D. L. Liu, A. Li, C. Z. Wang and Y. J. Wei, *J. Alloys Compd.*, 2009, **479**, 652; (*d*) T. Li, L. Li, Y. L. Cao, X. P. Ai and H. X. Yang, *J. Phys. Chem. C*, 2010, **114**, 3190.

5 (*a*) D. S. Wang, R. Xu, X. Wang and Y. D. Li, *Nanotechnology*, 2006, **17**, 979; (*b*) G. Mattei, P. Mazzoldi, M. L. Post, D. Buso, M. Guglielmi and A. Martucci, *Adv. Mater.*, 2007, **19**, 561; (*c*) V. S. Maceira, M. A. C. Duarte, M. B. Lopez, M. Grzelczak, M. Farle, L. M. L. Marzan and J. Rivas, *Adv. Funct. Mater.*, 2008, **18**, 616; (*d*) H. Liu, G. X. Wang, J. Liu, S. Z. Qiao and H. Ahnc, *J. Mater. Chem.*, 2011, **21**, 3046; (*e*) S. A. Needham, G. X. Wang and H. K. Liu, *J. Power Sources*, 2006, **159**, 254; (*f*) Y. Q. Zou and Y. Wang, *Nanoscale*, 2011, **3**, 2615; (*g*) I. R. M. Kottegoda, N. H. Idrisa, L. Lu, J. Z. Wang and H. K. Liu, *Electrochim. Acta*, 2011, **56**, 5815.

6 (*a*) S. M. Paek, E. J. Yoo and I. Honma, *Nano Lett.*, 2009, **9**, 72; (*b*) D. h. Wang, D. W. Choi, J. Li, Z. G. Yang, Z. M. Nie, R. Kou, D. H. Hu, C. M. Wang, L. V. Saraf, J. G. Zhang, I. A. Aksay and J. Liu, *ACS Nano*, 2009, **3**, 907; (*c*) Z. S. Wu, W. C. Ren, L. Wen, L. B. Gao, J. P. Zhao, Z. P. Chen, G. M. Zhou, F. Li and H. M. Cheng, *ACS Nano*, 2010, **4**, 3187; (*d*) X. J. Zhu, Y. W. Zhu, S. Murali, M. D. Stoller and R. S. Ruoff, *ACS Nano*, 2011, **5**, 3333; (*e*) H. L. Wang, L. F. Cui, Y. Yang, H. S. Casalongue, J. T. Robinson, Y. Liang, Y. Cui and H. J. Dai, *J. Am. Chem. Soc.*, 2010, **132**, 13978; (*f*) Y. Q. Sun, Q. Wu and G. Q. Shi, *Energy Environ. Sci.*, 2011, **4**, 1113; (*g*) M. Pumera, *Energy Environ. Sci.*, 2011, **4**, 668.

7 (*a*) W. S. Hummers and R. E. Offeman, *J. Am. Chem. Soc.*, 1958, **80**, 1339; (*b*) X. L. Li, X. R. Wang, L. Zhang, S. Lee and H. J. Dai, *Science*, 2008, **319**, 1229; (*c*) K. S. Novoselov, A. K. Geim, S. V. Morozov, D. Jiang, M. I. Katsnelson, I. V. Grigorieva, S. V. Dubonos and A. A. Firsov, *Nature*, 2005, **438**, 197; (*d*) J. C. Meyer, A. K. Geim, M. I. Katsnelson, K. S. Novoselov, T. J. Booth and S. Roth, *Nature*, 2007, **446**, 60; (*e*) D. A. Dikin, S. Stankovich, E. J. Zimney, R. D. Piner, G. H. B. Dommett, G. Evmenenko, S. T. Nguyen and R. S. Ruoff, *Nature*, 2007, **448**, 457.

8 (*a*) X. Y. Wang, X. F. Zhou, K. Yao, J. G. Zhang and Z. P. Liu, *Carbon*, 2011, **49**, 133; (*b*) Y. J. Mai, X. L. Wang, J. Y. Xiang, Y. Q. Qiao, D. Zhang, C. D. Gu and J. P. Tu, *Electrochim. Acta*, 2011, **56**, 2306.

9 S. J. Ding, D. Luan, F. Y. C. Boey, J. S. Chen and X. W. Lou, *Chem. Commun.*, 2011, **47**, 7155.

10 J. C. Hu, K. Zhu, L. F Chen, H. J. Yang, Z. Li, A. Suchopar and R. Richards, *Adv. Mater.*, 2008, **20**, 267.